



Published in final edited form as:

*Cancer Res.* 2009 April 1; 69(7): 2801–2808. doi:10.1158/0008-5472.CAN-08-4051.

## Endothelial nitric oxide synthase mediates lymphangiogenesis and lymphatic metastasis

Johanna Lahdenranta<sup>1</sup>, Jeroen Hagendoorn<sup>1</sup>, Timothy P. Padera, Tohru Hoshida, Gregory Nelson, Satoshi Kashiwagi, Rakesh K. Jain, and Dai Fukumura

*Edwin L. Steele Laboratory, Department of Radiation Oncology, Massachusetts General Hospital and Harvard Medical School, Boston, Massachusetts, 02114, USA.*

### Abstract

Lymphatic metastasis is a critical determinant of cancer prognosis. Recently, several lymphangiogenic molecules such as vascular endothelial growth factor (VEGF)-C and -D were identified. However, the mechanistic understanding of lymphatic metastasis is still in infancy. Nitric oxide (NO) plays a crucial role in regulating blood vessel growth and function as well as lymphatic vessel function. NOS expression correlates with lymphatic metastasis. However, causal relationship between NOS and lymphatic metastasis has not been documented. To this end, we first show that both VEGF receptor-2 and -3 stimulation activate eNOS in lymphatic endothelial cells and that NO donors induce proliferation and/or survival of cultured lymphatic endothelial cells in a dose dependent manner. We find that an NOS inhibitor L-NMMA blocked regeneration of lymphatic vessels. Using intravital microscopy that allows us to visualize the steps of lymphatic metastasis, we show that genetic deletion of eNOS as well as NOS blockade attenuates peritumor lymphatic hyperplasia of VEGF-C-overexpressing T241 fibrosarcomas and decreases the delivery of metastatic tumor cells to the draining lymph nodes. Genetic deletion of eNOS in the host also leads to a decrease in T241 tumor cell dissemination to the lymph nodes and macroscopic lymph node metastasis of B16F10 melanoma. These findings indicate that eNOS mediates VEGF-C induced lymphangiogenesis and, consequently, plays a critical role in lymphatic metastasis. Our findings explain the correlation between NOS and lymphatic metastasis seen in a number of human tumors and open the door for potential therapies exploiting NO signaling to treat diseases of the lymphatic system.

### Keywords

nitric oxide; lymphangiogenesis; lymphatic metastasis; intravital microscopy; VEGF-C

### Introduction

NO mediates an array of physiological and pathological processes including the formation and function of blood vessels as well as the growth and dissemination of tumors via blood vessels (1). There are three isoforms of NO synthase (NOS): neuronal NOS (nNOS), inducible NOS (iNOS) and endothelial NOS (eNOS). In blood vessels, NO derived from eNOS mediates vascular function, angiogenesis and vessel maturation (1). Perivascular NO gradients can normalize structural and functional abnormalities of tumor vasculature (2). eNOS is also

*To whom correspondence may be addressed at:* Dai Fukumura or Rakesh K. Jain, Edwin L. Steele Laboratory for Tumor Biology, Department of Radiation Oncology, Massachusetts General Hospital and Harvard Medical School, 100 Blossom Street - Cox 7, Boston MA 02114, e-mail: E-mail: dai@steele.mgh.harvard.edu or E-mail: jain@steele.mgh.harvard.edu.

<sup>1</sup>These authors contributed equally to this work

expressed in the lymphatic system (3) and affects microlymphatic fluid flow by acting on collecting lymphatics (4). A positive correlation between NOS expression/activity in tumor tissues and lymphatic metastasis has been demonstrated in head and neck, thyroid, breast, stomach, gallbladder cancers (reviewed in (1) and melanoma (5). Blocking NO signaling through soluble guanylate cyclase has also been recently shown to reduce UVB irradiation induced lymphatic hyperplasia (6). These studies suggest that NO signaling mediates lymphangiogenesis *in vivo*. However, it remains unknown whether NOS plays a causal role in lymphangiogenesis during wound healing and lymphatic metastasis (7).

The lymphatic vascular system is a network of endothelium-lined vessels that absorbs and transports interstitial fluid, in addition to lymphocytes and antigen presenting cells, to lymph nodes (8). The lymphatic system also transports metastatic cancer cells to lymph nodes (9). Vascular endothelial growth factor (VEGF)-C and D, acting via activation of the lymphatic endothelial VEGFR-3, were identified as the first lymphangiogenic factors (reviewed in (10). Tumors overexpressing VEGF-C exhibit increased lymphatic vessel density and lymphatic hyperplasia, and an increased rate of lymphatic metastasis as a result of abnormal formation and enlargement of peritumor lymphatics (9,11,12). In this study, we explore whether NOS plays a causal role in VEGF-C induced lymphangiogenesis, lymphatic hyperplasia and lymphatic metastasis in this setting.

Here, we use *in vitro* and *in vivo* models to dissect the role of NO on lymphangiogenesis. First, we assess the ability of VEGFR-2 and VEGFR-3 ligands to activate eNOS in cultured LECs and the ability of NO to stimulate the growth of LECs grown in culture. Next, we assess the effect of NOS-blockade with L-NMMA on lymphangiogenesis in collagen implants in a model of dermal regeneration in the mouse tail. Finally, we assess the effect of pharmacological or genetic blockade of NOS on peritumor lymphatic hyperplasia in VEGF-C-overexpressing T241 fibrosarcomas and B16F10 melanomas implanted in the mouse ear. In this model, we also quantify the number of metastatic tumor cells arriving in the draining lymph node or alternatively, the presence of macroscopic metastasis. Our results provide the first direct evidence that eNOS mediates VEGF-C induced lymphangiogenesis, peritumor lymphatic hyperplasia and lymphatic metastasis.

## Materials and Methods

### Cells, antibodies and growth factors

Neonatal Human Dermal Lymphatic Microvascular Endothelial Cells (LECs) were obtained from Cambrex. LECs were cultured in complete EGM-2 MV media on human fibronectin (fn, 1  $\mu\text{g}/\text{cm}^2$ ; BD Biosciences) coated flasks. T241 fibrosarcoma cell line stably overexpressing VEGF-C and engineered to constitutively express GFP (T241-VEGF-C-GFP) has been described (9). Akt, Phospho-Akt (Ser473), p42/p44, Phospho-p42/p44 (Thr202/Tyr204) and Phospho-eNOS (Ser1177) antibodies were from Cell Signaling Technologies (used 1:1000 for Western Blot – analysis), eNOS and iNOS antibodies from BD Transduction Laboratories (used 1:2500 for Western Blot analysis and 1:1000 for eNOS and 1:200 for iNOS IHC analysis), MECA-32 (used 1:200 for IHC analysis) antibody from BD Pharmingen, LYVE-1 antibody (used 1:2000 for IHC analysis) from Upstate Cell Signaling Solutions and proliferating cell nuclear antigen (PCNA; Ready-to-use solution, used 1:5 for IHC analysis) antibody from DAKO. Recombinant human (rh) VEGF-A, VEGF-C wt and VEGF-C (*Cys156Ser*) were from R&D Systems.

### Cell proliferation assay

LECs were seeded in fibronectin (1  $\mu\text{g}/\text{cm}^2$ , Sigma) coated microtiter wells (3500 cells/well) and starved in EGM-2 media supplemented with hydrocortisone, ascorbic acid, gentamicin,

amphotericin-B (according to manufacturer's instructions) and 1% FBS (starving media) for 16–20h. Media was changed to full media (EGM-2 MV containing 5% FBS) or starving media containing increasing concentrations of (Z)-1-[N-(2-aminoethyl)-N-(2-ammonioethyl)amino] diazen-1-ium-1,2-diolate (DETA-NONOate) or [N-(2-Deoxy- $\alpha$ , $\beta$ -D-glucopyranose-2-)-N<sup>2</sup>-acetyl-S-nitroso-D,L-penicillaminamide] (Glyco-SNAP-2, Alexis Biochemicals). Cells were incubated at 37°C in 5% CO<sub>2</sub> for 72 h. Cell proliferation was assessed by measuring the ability of cells to metabolize the tetrazolium salt WST-1 (Roche) to formazan in a colorimetric assay.

### Growth factor stimulation and Western blot analysis

LECs in fibronectin coated plates were starved for 18–24 hours. Cells were stimulated for 30 minutes with rhVEGF-A (50 ng/ml), rhVEGF-C wt (200 ng/ml) or rhVEGF-C (*Cys156Ser*). In a separate set of experiments, stimulation was preceded by a 2 hour incubation with 30nM Wortmannin (Calbiochem/EMD) or 10 $\mu$ M U0126 (Cell Signaling Technology). Cells were lysed in RIPA-buffer (50 mM Tris-HCl, pH 7.4, 150 mM NaCl, 1% NP-40, 0.1% SDS, protease and phosphatase inhibitors). Equal amounts of protein (quantified using DC Protein Assay, BioRad) were separated by SDS-PAGE and transferred to PVDF membrane and immunoblotted with the specified antibodies using HRP-conjugated secondary antibodies (1:7500 dilution, GE Healthcare Life Sciences/ Amersham Biosciences) and enhanced chemiluminescence detection system (ECL, GE Healthcare Life Sciences, Amersham Biosciences).

### Animals

*In vivo* studies were performed in 8–12 week old FVB mice, *Tie2 promoter driven-green fluorescent protein (GFP)/FVB* mice, nude mice, C57Bl/6 mice or *eNOS*<sup>-/-</sup> (13) in C57Bl/6 background. All mice were bred and maintained at Massachusetts General Hospital (MGH). All procedures were performed following the guidelines of Public Health Service Policy on Humane Care of Laboratory Animals and approved by the Institutional Animal Care and Use Committee of the MGH.

### Lymphangiogenesis in the mouse tail

A model developed by Dr. Melody Swartz and colleagues that allows intravital microscopy of lymphangiogenesis in a collagen construct in the mouse tail was used (14). Briefly, a 2-mm-wide, circumferential segment of skin and subcutis was removed using microsurgical dissection thereby removing all lymphatics and leaving only the major blood vessels, tendons, muscle, and bone intact. The collecting lymphatics running alongside the tail veins (4) were identified and severed. A 0.35% type I rat tail collagen solution (BD Biosciences) was injected in the defect and kept in place for 20–25 days by a silicon sleeve (silastic tubing ID 3.35mm/OD 4.65mm; Dow Corning) fixed with tissue adhesive (Nexaband S/C, Abbott Laboratories). The use of multiphoton laser-scanning microscopy (MPLSM) and lymphangiography has been described previously (11). To concurrently image angiogenesis and lymphangiogenesis in the tail collagen construct, FVB and *Tie2<sup>P</sup>-GFP/FVB* mice (n = 9) were anesthetized and lymphangiography was performed using 10 mg/ml TAMRA-Dextran (2M MW, Molecular Probe) or 2.5 mg/ml FITC-Dextran (Sigma). MPLSM was performed to image angiogenesis and lymphangiogenesis between 25 and 70 days after collagen construct implantation.

### Peritumor lymphangiogenesis and lymph node metastasis

We used a tumor model that allows *in vivo* functional lymphangiography and multiphoton microscopy of peritumor lymphatics and the lymph node draining the tumor to study the effect of NOS inhibition on each step of lymphatic metastasis (15). Briefly, a suspension of T241-VEGF-C-GFP cells was injected in the peripheral ear. At day 7 or day 14 after tumor implantation, lymphangiography was performed in anesthetized mice by injection of 2 $\mu$ l 10

mg/ml TAMRA-Dextran in the surface of tumors. Peritumor lymphatic diameters were quantified with ImageJ software using images obtained by intravital fluorescence microscopy. Seven or 14 days after implantation, tumor cell arrival in the cervical lymph node was quantified as described before (9). Following lymphangiography of the peripheral ear with TAMRA-Dextran, all GFP+ tumor cells in the exposed cervical lymph node were imaged using multiphoton laser-scanning microscopy. The number of cells per lymph node was hand-counted in single-stack images using ImageJ software by a blinded observer.

### **NO inhibition *in vivo***

Production of NO was lowered by administering the NOS inhibitor L-NMMA (350 mg/kg/day) via a subcutaneous osmotic pump as described (4). This dose of L-NMMA does not induce arterial hypertension (4). Angiogenesis precedes lymphangiogenesis during wound healing. We started L-NMMA treatments after the initial period of angiogenesis to minimize the interference on angiogenesis. FVB mice received L-NMMA (n = 4) or PBS (n = 6) starting 21 days after the collagen gel was implanted in the tail. At day 60, lymphangiography and single-photon microscopy of the full circumference of the tail were performed. Nude mice received L-NMMA (n = 8) or PBS (n = 8) starting 7 days after implantation of T241-VEGF-C-GFP cells in the ear. Lymphangiography of the ear was performed prior to L-NMMA treatment on day 7 and was repeated on day 14 after 7 days of NOS inhibition. MPLSM imaging of the cervical lymph node was also performed on day 14 (L-NMMA treated animals) or around day 7 (in wt or eNOS<sup>-/-</sup> mice when tumors had reached approximately 80–90 mm<sup>3</sup> in size), to detect metastatic GFP+ tumor cells as described above. It has been shown that L-NMMA promotes oxygen radical production by eNOS (uncoupling) *in vitro* under the lack of eNOS substrate/cofactors (16). In order to avoid both off-target effects of L-NMMA and to distinguish the effects of NO synthesized by eNOS from the effects of reactive oxygen species production, as well as to confirm that the observed effects of NOS inhibitors are specifically due to the inhibition of the endothelial isoform of NOS, we performed our studies on tumor-induced lymphatic hyperplasia and lymphatic metastasis in eNOS knockout animals.

### **Immunohistochemistry (IHC)**

IHC was performed for MECA-32, LYVE-1, and PCNA as described previously (11). Tumor vascular endothelial cell density was quantified using MECA-32 (17). IHC was performed for eNOS and iNOS as described before (17). Serial sections stained for LYVE-1 and PCNA were used to determine the number of proliferating lymphatic endothelial cells per vessel cross section; serial sections stained for LYVE-1 and eNOS/iNOS were used to confirm the presence of NOS isoforms on peritumor lymphatics. Quantification of the perimeter/diameter of peritumor lymphatics has been described (18).

### **Statistics**

Results are presented as mean ± SEM. Student *t* test, Fisher's exact test and Mann-Whitney-U-test (where noted) were used to evaluate statistical significance (defined as  $P < 0.05$ ). Equality of variances was evaluated using *F* test.

## **Results and Discussion**

### **VEGF-C activates eNOS in lymphatic endothelial cells through PI3K pathway**

Activation of VEGFR-2 increases production of NO in blood vascular endothelial cells via activation of eNOS (19). A number of intracellular molecules mediate eNOS activation in blood vascular endothelial cells, including calcium, the PI3K/Akt, heat-shock protein 90 and phospholipase C- $\gamma$  (PLC, reviewed in (20)). Interestingly, both the PI3K/Akt cascade (21) and PLC (22) are induced by VEGF-C/VEGFR-3 signaling, suggesting a possible downstream

dependence of VEGFR-3 signaling on nitric oxide. In order to determine whether activation of VEGFR-3 by VEGF-C and the following downstream signaling events can lead to activation of eNOS in LECs, we studied the activation of eNOS in response to angiogenic and lymphangiogenic stimuli in LECs. First, LECs were stimulated with full growth media, VEGF-A, VEGF-C or VEGF-C156S (VEGFR-3 specific variant; (23)). We examined eNOS activation by western blot analysis with a phospho-eNOS (Ser1177) specific antibody, and found eNOS to be activated in response to VEGF-A and VEGF-C stimulation. In addition, the VEGFR-3 specific form of VEGF-C (VEGFC156S) led to eNOS activation, establishing that VEGFR-3 activation alone is sufficient for the activation of eNOS in LECs (Fig. 1A).

Intracellular molecules mediating VEGF-C-induced eNOS activation in LECs have remained unidentified. Since PI3K/Akt signaling pathway is known to be activated upon VEGFR-3 stimulation in LECs (21), we tested whether this pathway has a role in the activation of eNOS in lymphatic endothelial cells. We examined Akt activation by western blot analysis with a phospho-Akt (Ser473) specific antibody, and found, as anticipated, that Akt was activated in response to VEGF-A, VEGF-C and VEGF-C156S stimulation (Fig 1A). In addition, pre-treatment of LECs with Wortmannin, a PI3K inhibitor, before the growth factor stimulation was able to partially block the activation of eNOS by preventing Akt activation (Fig. 1A), establishing that eNOS activation through VEGFR-2 and -3 signaling is dependent on PI3K mediated Akt activation. In contrast, MEK1/2 Inhibitor U0126 did not block eNOS activation in LECs (Fig. 1A). Since p42/p44 has been indicated in the eNOS activation, we examined its activation in LECs by western blot analysis with a phospho-p42/p44 (Thr202/Tyr204) specific antibody, and found that p42/p44 was activated in response to VEGF-C and VEGF-C156S stimulation (Fig. 1A). In summary, we show that stimulation of LECs through either VEGFR-2 or VEGFR-3 leads to a PI3K dependent activation of eNOS. However, there might be other downstream signaling pathways from VEGFR-2 and VEGFR-3 that further modulate eNOS activity.

### **NO donors stimulate lymphatic endothelial cell proliferation and/or survival**

We assessed the effects of two structurally different slow releasing NO donors on LEC proliferation and/or survival *in vitro*. LECs were subjected to increasing concentrations of either DETA NONOate ( $t_{1/2}$  of release 20h) or Glyco-SNAP-2 ( $t_{1/2}$  of release 24h). After 72 hours, proliferation of LECs was assessed by a colorimetric assay with WST-1. DETA-NONOate and Glyco-SNAP-2 significantly induced proliferation and/or survival of LECs in a dose dependent manner from 50  $\mu$ M to 500  $\mu$ M ( $P < 0.05$ ; Fig. 1B). Glyco-SNAP-2 had no significant effect on cell proliferation at 1000  $\mu$ M, possibly due to Glyco-SNAP-2 toxicity to LECs (Figure 1B). In agreement with the recent report (5), these data suggest that NO stimulates the proliferation and/or survival of microvascular lymphatic endothelial cells.

### **NOS-inhibition blocks lymphangiogenesis in dermal regeneration mouse-tail model**

We next assessed the effect of NOS inhibition on lymphangiogenesis using a dermal regeneration model in mouse tail (14). This model allows intravital microscopy of lymphangiogenesis (9) in a collagen construct where growth of new lymphatic vessels occurs from the distal to proximal direction between days 25 and 60 after implantation and depends on VEGF-C/VEGFR-3-signaling (24). A circumferential segment of skin and subcutis was removed and filled with type I collagen (14). To obtain high-resolution images of angiogenic and lymphangiogenic vessels in the collagen construct, we performed lymphangiography and multiphoton laser-scanning microscopy (MPLSM) in *Tie2 promoter driven-green fluorescent protein (Tie2<sup>P</sup>-GFP)/FVB* mice (constitutively expressing GFP in blood endothelial cells) between days 35 and 70 (Fig. 2A). Consistent with previous observations (14), lymphatic sprouting occurred in the distal margin of the construct at day 35 and subsequently expanded in the proximal direction (Fig. 2B). At day 60, newly regenerated lymphatics had formed in

the characteristic hexagonal pattern of the mouse-tail and multiple small sprouts (Fig. 2C), and nearly reached the proximal margin. Lymphatic regeneration detected by lymphangiography was heterogeneous, with the number of hexagon segments between 10 and 70% of that in normal tail skin. The newly formed lymphatics did not expand after day 70 and were stable for up to one year (Fig. 2D). Consistent with previous work *Tie2<sup>P</sup>*-GFP expression was not detectable on the microlymphatics of these mice (25), possibly because Tie2 promoter activity in lymphatics was below the detection limit of the GFP reporter by multiphoton microscopy (26).

To assess whether NOS is involved in lymphangiogenesis, we performed lymphangiography and intravital microscopy in mice that received an NOS inhibitor L-NMMA between days 21 and 60 after implantation of the collagen construct (n=4) and mice that received vehicle (PBS) alone (n=6). While 83.3% of the control mice exhibited growth of new lymphatics by 60 days after the wound creation, none of the mice treated with an NOS inhibitor L-NMMA showed functional lymphatics in the implanted collagen construct at the same time ( $p < 0.05$ , Fisher's exact test; Fig. 2E, F). Instead, fluorescent tracer diffused through certain areas of the regenerating region (not shown). The lymphatics distal and proximal to the construct appeared to function normally and none of the mice developed edema. Since the blood vasculature in this model is completely regenerated within 21 days of collagen implantation (14), the effect of NOS-inhibition on angiogenesis did not contribute to this study.

These data suggest that NOS mediates lymphangiogenesis in the model of dermal regeneration. Interestingly, in agreement with our findings, a previous study showed administration of cavtratin, which blocks eNOS activity, reduces intratumor density of VEGFR-3 expressing cells (27). Possibly, this was due to an anti-lymphangiogenic effect of eNOS-blockade, although this study did not further specify whether these cells were lymphatic endothelial cells (7).

### Pharmacologic and genetic inhibition of eNOS attenuates peritumor lymphatic hyperplasia

We have shown that overexpression of VEGF-C in T241 fibrosarcomas leads to hyperplasia of the peritumor lymphatic vessels without affecting growth of the primary tumor (9,11). Observed lymphatic hyperplasia was associated with an increased lymph flow rate and increased delivery of metastatic tumor cells in the cervical lymph node as compared with wild-type tumors (9,11). Using a pharmacological NOS inhibitor L-NMMA as well as a genetic inactivation of eNOS, we investigated the role of NOS in peritumor lymphatic hyperplasia in VEGF-C overexpressing tumors.

We used a model that allows *in vivo* functional lymphangiography and multiphoton microscopy of peritumor lymphatics and the draining lymph node on each step of lymphatic metastasis (9). Nude mice were implanted with T241 fibrosarcoma cells constitutively expressing VEGF-C and GFP (T241-VEGF-C-GFP). Mice received L-NMMA (n=8) or PBS (n=8) beginning 7 days after tumor implantation. Prior to the start of NOS-inhibition, the mean lymphatic vessel diameter of peritumor lymphatics was  $88.3 \pm 3.8 \mu\text{m}$  as determined by lymphangiography. After 7 days of L-NMMA treatment (14 days after tumor implantation), the mean lymphatic vessel diameter did not increase in the L-NMMA treated group, whereas a 46% increase was observed in controls ( $94 \pm 4 \mu\text{m}$  and  $137 \pm 12 \mu\text{m}$ ,  $P < 0.05$ ; Figures 3A, B and C). There was no difference in tumor size between the L-NMMA and control groups after 7 days of treatment (Table 1). LYVE-1 immunohistochemistry (IHC) confirmed that peritumor lymphatics in L-NMMA treated animals had a significantly smaller perimeter than controls ( $P < 0.05$ ; Table 1). In agreement with our previous studies (4), peritumor lymphatics expressed eNOS (Fig. 3D, E) but not iNOS (Supplementary Figure 1). The peritumor lymphatics in L-NMMA treated animals contained fewer proliferating endothelial cells per vessel cross section than controls ( $P < 0.05$ ; Table 1). In addition, intratumor blood vessel endothelial cell density in these tumors

assessed by MECA-32 immunohistochemistry was not affected by this L-NMMA treatment schedule (Table 1). Thus, the effect of NO on lymphatic vessels cannot be explained solely by a secondary phenomenon of the effect on blood vessels in our experimental models.

To delineate that the observed reduction in lymphatic hyperplasia was attributable to the inhibition of the endothelial isoform of NOS, *eNOS*<sup>-/-</sup> (n=6) or wild type (WT; C57Bl/6) mice (n=6) were implanted with T241-VEGF-C-GFP tumors. Tumor growth rates were similar in *eNOS*<sup>-/-</sup> and WT mice (data not shown). When tumors reached approximately 80 mm<sup>3</sup> in size (7–8 days after implantation), peritumoral lymphatics were visualized by lymphangiography. Normal ear lymphatic vessels had similar diameters in WT and *eNOS*<sup>-/-</sup> animals (74.2 ± 4.2 μm and 78.5 ± 3.5 μm, *P* = 0.5) whereas WT animals had significantly more peritumoral lymphatic hyperplasia when compared to *eNOS*<sup>-/-</sup> mice (lymphatic diameters 116.1 ± 3.9 μm and 98.4 ± 6.2 μm, *P* < 0.05; Fig. 3D). Interestingly, the peritumor lymphatic diameters in the L-NMMA treated and *eNOS*<sup>-/-</sup> animals were similar to that in non-VEGF-C overexpressing tumors, VEGFR-3 neutralizing-antibody treated VEGF-C overexpressing tumors (9) or the tyrosine kinase inhibitor cediranib (28). Taken together, these results show that eNOS-blockade attenuates peritumor lymphatic endothelial cell proliferation and peritumor lymphatic vessel hyperplasia associated with VEGF-C overexpressing tumors. Similar results of L-NMMA treatment and eNOS null mice experiments suggest that the effect of L-NMMA is dominated by ordinal eNOS inhibition and not eNOS uncoupling in our study.

In addition to NO production by lymphatic endothelial cells, other sources of NO production are possible. Tumor cells can produce NO through genetic and environmental upregulation of NOSs (1). However, our immunohistochemical analysis suggests that tumor cells do not produce eNOS or iNOS appreciably in the model used in this study. Macrophages and fibroblasts can be activated in tumors and lead to iNOS induction and NO production. Another potential source of NO in the tumors is blood vascular endothelium. NO produced by these cells may provide a lymphangiogenic signal required for lymphatic regeneration and peritumor lymphatic hyperplasia. Blockade of this source of NO would also lead to the results seen in our experiments. Interestingly, several recent studies suggest that iNOS-derived NO may increase production of VEGF-C and/or VEGF-D in tumor cells and thus, contribute to lymphangiogenesis and lymph node metastasis (29–31). Since VEGF-C is under a constitutive promoter and is produced at much higher levels than in the mock transduced cells in our experiments, iNOS derived NO is unlikely to influence the levels of tumor cell produced VEGF-C. Nevertheless, through differential effects on tumor cells, stroma and vasculature, NO has a complex roles in carcinogenesis, tumor progression and metastasis (1).

### **NOS-inhibition decreases arrival of metastatic tumor cells in the lymph node and macroscopic metastasis**

Peritumor lymphatic hyperplasia induced by VEGF-C increases the opportunity of tumor cells to enter the lymphatics (9,32) and increases intralymphatic transport of fluid to the lymph node (9,33). Reduction of peritumor lymphatic hyperplasia by NOS-blockade could thus lead to decreased delivery of tumor cells to lymph node and thus, fewer lymph node metastases. To test this hypothesis, we directly imaged metastatic T241-VEGF-C-GFP cells that spontaneously spread to the cervical lymph node from ear tumors using multiphoton microscopy (Fig. 4A). We first used L-NMMA to inhibit NOS activity and found that number of GFP-positive tumor cells in the draining cervical lymph node at day 14 after tumor implantation was significantly decreased in L-NMMA treated (from days 7 to 14) animals compared to control animals (*P* < 0.05; Fig 4B). Similar decreases in tumor cell arrival were previously observed in the same tumor model with VEGFR-3 neutralizing antibody treatment and the tyrosine kinase inhibitor cediranib (9,28). Next, we imaged metastatic T241-VEGF-C-GFP cells spreading to the cervical lymph node from ear tumors in wild type and *eNOS*<sup>-/-</sup>

mice. When tumors had reached approximately 80–90 mm<sup>3</sup> in size, the number of GFP-positive tumor cells in the draining cervical lymph node after tumor implantation was significantly decreased in *eNOS*<sup>-/-</sup> animals (n=8) compared to wild type animals (n=6; 107.5 ± 38.1 and 330.3 ± 75.4 tumor cells/lymph node, *P* < 0.05, Mann-Whitney-U-test; Fig 4B). These data suggest that inhibition of peritumor lymphatic hyperplasia by NOS-blockade or genetic deletion of eNOS decreases the number of metastatic cells arriving in the lymph node.

Finally, we used a syngeneic B16F10 tumor model in *eNOS*<sup>-/-</sup> and wild type mice to address whether genetic deletion of eNOS in the lymphatic vessels affects peritumor hyperplasia and the formation of clinical metastasis in a tumor model without artificial overexpression of VEGF-C. *eNOS*<sup>-/-</sup> or wild type mice were implanted with B16F10 tumors. When tumors reached approximately 80–100 mm<sup>3</sup> in size, primary tumors were resected and processed for immunohistochemical analysis. 14 days after resection of the primary tumors the number of draining cervical lymph nodes with metastatic lesions was significantly higher in wild type mice than in *eNOS*<sup>-/-</sup> mice (9/14 LN positive and 2/14 LN positive, *P* < 0.05, Fisher's exact test; Fig. 4C). While statistically non-significant, we observed a trend towards smaller diameters of LYVE1+ peritumoral lymphatic vessels in *eNOS*<sup>-/-</sup> mice when compared to wild type mice (22.6 ± 2.9 μm and 26.2 ± 1.6 μm, *P* = 0.3 Fig. 4D). Diameters of peritumoral blood vessels were similar in *eNOS*<sup>-/-</sup> and wild type mice (6.4 ± 0.7 μm and 5.8 ± 0.4 μm, *P* = 0.4).

In summary, we show that inhibiting eNOS activity either genetically or pharmacologically significantly reduces the number of tumor cells arriving to the tumor draining lymph node and the subsequent formation of macroscopic metastasis. Since NOS inhibition reduced the number of cancer cells delivered to the draining lymph nodes, our data suggest that NO participates in the earliest steps of lymphatic metastasis. As NOS inhibition can also inhibit tumor growth, likely through an antiangiogenic mechanism, the use of NOS inhibition may prove a useful adjuvant therapy for metastatic disease. Both the further spread of cancer cells from the tumor bed to the lymph node and the growth of those cells in lymph nodes could be reduced by NOS inhibition.

We show here for the first time a causal relationship between NOS, lymphangiogenesis and lymphatic metastasis. It is attractive to think that treatments that block NO production and signaling could simultaneously block tumor associated angiogenesis and reduce lymphatic metastasis. Future investigations will need to determine the importance of the relative contributions of VEGFR-2 and VEGFR-3 and the different NOS isoforms (eNOS, iNOS, nNOS) to lymphangiogenesis and lymphatic metastasis. In addition, determining the target cells producing NO will be important in therapeutic design. Our novel findings add NO to the growing list of lymphangiogenic molecules and open the door for potential therapies exploiting NO signaling to treat diseases of the lymphatic system, including lymphatic metastasis and lymphedema.

## Supplementary Material

Refer to Web version on PubMed Central for supplementary material.

## Acknowledgments

The authors would like to thank Ms. Sylvie Roberge, Julia Kahn, and Carolyn Smith for excellent technical support; Drs. Melody Swartz and Jeremy Goldman for generous help with the tail lymphangiogenesis model, Dr. Paul L. Huang for *eNOS*<sup>-/-</sup> mice and Drs. Angera Kuo and Shan Liao for helpful discussions. This work was supported by NIH Grant R01-CA85140 (RKJ) and R01-CA96915 (DF). JL is a Robert Black Fellow of the Damon Runyon Cancer Research Foundation (DRG-1904-06).

*Grant support:* National Cancer Institute grants R01-CA85140 (R.K. Jain) and R01-CA96915 (D. Fukumura). J Lahdenranta is a Robert Black Fellow of the Damon Runyon Cancer Research Foundation (DRG-1904-06).

## References

1. Fukumura D, Kashiwagi S, Jain RK. The role of nitric oxide in tumour progression. *Nat Rev Cancer* 2006;6:521–534. [PubMed: 16794635]
2. Kashiwagi S, Tsukada K, Xu L, et al. Perivascular nitric oxide gradients normalize tumor vasculature. *Nat Med* 2008;14:255–257. [PubMed: 18278052]
3. Marchetti C, Casasco A, Di Nucci A, et al. Endothelin and nitric oxide synthase in lymphatic endothelial cells: immunolocalization in vivo and in vitro. *Anat Rec* 1997;248:490–497. [PubMed: 9268139]
4. Hagendoorn J, Padera TP, Kashiwagi S, et al. Endothelial nitric oxide synthase regulates microlymphatic flow via collecting lymphatics. *Circ Res* 2004;95:204–209. [PubMed: 15192027]
5. Massi D, De Nisi MC, Franchi A, et al. Inducible nitric oxide synthase expression in melanoma: implications in lymphangiogenesis. *Mod Pathol*. 2008
6. Kajiya K, Huggenberger R, Drinnenberg I, Ma B, Detmar M. Nitric oxide mediates lymphatic vessel activation via soluble guanylate cyclase alpha1beta1-impact on inflammation. *FASEB J* 2008;22:530–537. [PubMed: 17855621]
7. Hagendoorn J, Padera TP, Fukumura D, Jain RK. Molecular regulation of microlymphatic formation and function: role of nitric oxide. *Trends Cardiovasc Med* 2005;15:169–173. [PubMed: 16165013]
8. Schmid-Schonbein GW. Microlymphatics and lymph flow. *Physiol Rev* 1990;70:987–1028. [PubMed: 2217560]
9. Hoshida T, Isaka N, Hagendoorn J, et al. Imaging steps of lymphatic metastasis reveals that vascular endothelial growth factor-C increases metastasis by increasing delivery of cancer cells to lymph nodes: therapeutic implications. *Cancer Res* 2006;66:8065–8075. [PubMed: 16912183]
10. Alitalo K, Tammela T, Petrova TV. Lymphangiogenesis in development and human disease. *Nature* 2005;438:946–953. [PubMed: 16355212]
11. Padera TP, Kadambi A, di Tomaso E, et al. Lymphatic metastasis in the absence of functional intratumor lymphatics. *Science* 2002;296:1883–1886. [PubMed: 11976409]
12. Achen MG, McColl BK, Stacker SA. Focus on lymphangiogenesis in tumor metastasis. *Cancer Cell* 2005;7:121–127. [PubMed: 15710325]
13. Huang PL, Huang Z, Mashimo H, et al. Hypertension in mice lacking the gene for endothelial nitric oxide synthase. *Nature* 1995;377:239–242. [PubMed: 7545787]
14. Boardman KC, Swartz MA. Interstitial flow as a guide for lymphangiogenesis. *Circ Res* 2003;92:801–808. [PubMed: 12623882]
15. Hoshida T, Isaka N, Hagendoorn J, et al. Imaging steps of lymphatic metastasis reveals that vascular endothelial growth factor-C increases metastasis by increasing delivery of cancer cells to lymph nodes: therapeutic implications. *Cancer Res* 2006;66:8065–8075. [PubMed: 16912183]
16. Forstermann U, Munzel T. Endothelial Nitric Oxide Synthase in Vascular Disease: From Marvel to Menace. *Circulation* 2006;113:1708–1714. [PubMed: 16585403]
17. Kashiwagi S, Izumi Y, Gohongi T, et al. NO mediates mural cell recruitment and vessel morphogenesis in murine melanomas and tissue-engineered blood vessels. *J Clin Invest* 2005;115:1816–1827. [PubMed: 15951843]
18. Hagendoorn J, Tong R, Fukumura D, et al. Onset of abnormal blood and lymphatic vessel function and interstitial hypertension in early stages of carcinogenesis. *Cancer Res* 2006;66:3360–3364. [PubMed: 16585153]
19. Fukumura D, Gohongi T, Kadambi A, et al. Predominant role of endothelial nitric oxide synthase in vascular endothelial growth factor-induced angiogenesis and vascular permeability. *Proc Natl Acad Sci U S A* 2001;98:2604–2609. [PubMed: 11226286]
20. Sessa WC. eNOS at a glance. *J Cell Sci* 2004;117:2427–2429. [PubMed: 15159447]
21. Makinen T, Veikkola T, Mustjoki S, et al. Isolated lymphatic endothelial cells transducer growth, survival and migratory signals via the VEGF-C/D receptor VEGFR-3. *EMBO J* 2001;20:4762–4773. [PubMed: 11532940]
22. Wang JF, Zhang X, Groopman JE. Activation of vascular endothelial growth factor receptor-3 and its downstream signaling promote cell survival under oxidative stress. *J Biol Chem* 2004;279:27088–27097. [PubMed: 15102829]

23. Joukov V, Kumar V, Sorsa T, et al. A recombinant mutant vascular endothelial growth factor-C that has lost vascular endothelial growth factor receptor-2 binding, activation, and vascular permeability activities. *J Biol Chem* 1998;273:6599–6602. [PubMed: 9506953]
24. Pytowski B, Goldman J, Persaud K, et al. Complete and specific inhibition of adult lymphatic regeneration by a novel VEGFR-3 neutralizing antibody. *J Natl Cancer Inst* 2005;97:14–21. [PubMed: 15632376]
25. Chang LK, Garcia-Cardena G, Farnebo F, et al. Dose-dependent response of FGF-2 for lymphangiogenesis. *Proc Natl Acad Sci U S A* 2004;101:11658–11663. [PubMed: 15289610]
26. Tammela T, Saariisto A, Lohela M, et al. Angiopoietin-1 promotes lymphatic sprouting and hyperplasia. *Blood* 2005;105:4642–4248. [PubMed: 15746084]
27. Gratton JP, Lin MI, Yu J, et al. Selective inhibition of tumor microvascular permeability by cavtratin blocks tumor progression in mice. *Cancer Cell* 2003;4:31–39. [PubMed: 12892711]
28. Padera TP, Kuo AH, Hoshida T, et al. Differential response of primary tumor versus lymphatic metastasis to VEGFR-2 and VEGFR-3 kinase inhibitors cediranib and vandetanib. *Mol Cancer Ther* 2008;7:2272–2279. [PubMed: 18687659]
29. Franchi A, Massi D, Santucci M, et al. Inducible nitric oxide synthase activity correlates with lymphangiogenesis and vascular endothelial growth factor-C expression in head and neck squamous cell carcinoma. *J Pathol* 2006;208:439–445. [PubMed: 16278821]
30. Nakamura Y, Yasuoka H, Tsujimoto M, et al. Nitric oxide in breast cancer: induction of vascular endothelial growth factor-C and correlation with metastasis and poor prognosis. *Clin Cancer Res* 2006;12:1201–1207. [PubMed: 16489074]
31. Nakamura Y, Yasuoka H, Zuo H, et al. Nitric oxide in papillary thyroid carcinoma: induction of vascular endothelial growth factor D and correlation with lymph node metastasis. *J Clin Endocrinol Metab* 2006;91:1582–1585. [PubMed: 16418215]
32. He Y, Rajantie I, Pajusola K, et al. Vascular endothelial cell growth factor receptor 3-mediated activation of lymphatic endothelium is crucial for tumor cell entry and spread via lymphatic vessels. *Cancer Res* 2005;65:4739–4746. [PubMed: 15930292]
33. Alitalo K, Carmeliet P. Molecular mechanisms of lymphangiogenesis in health and disease. *Cancer Cell* 2002;1:219–227. [PubMed: 12086857]

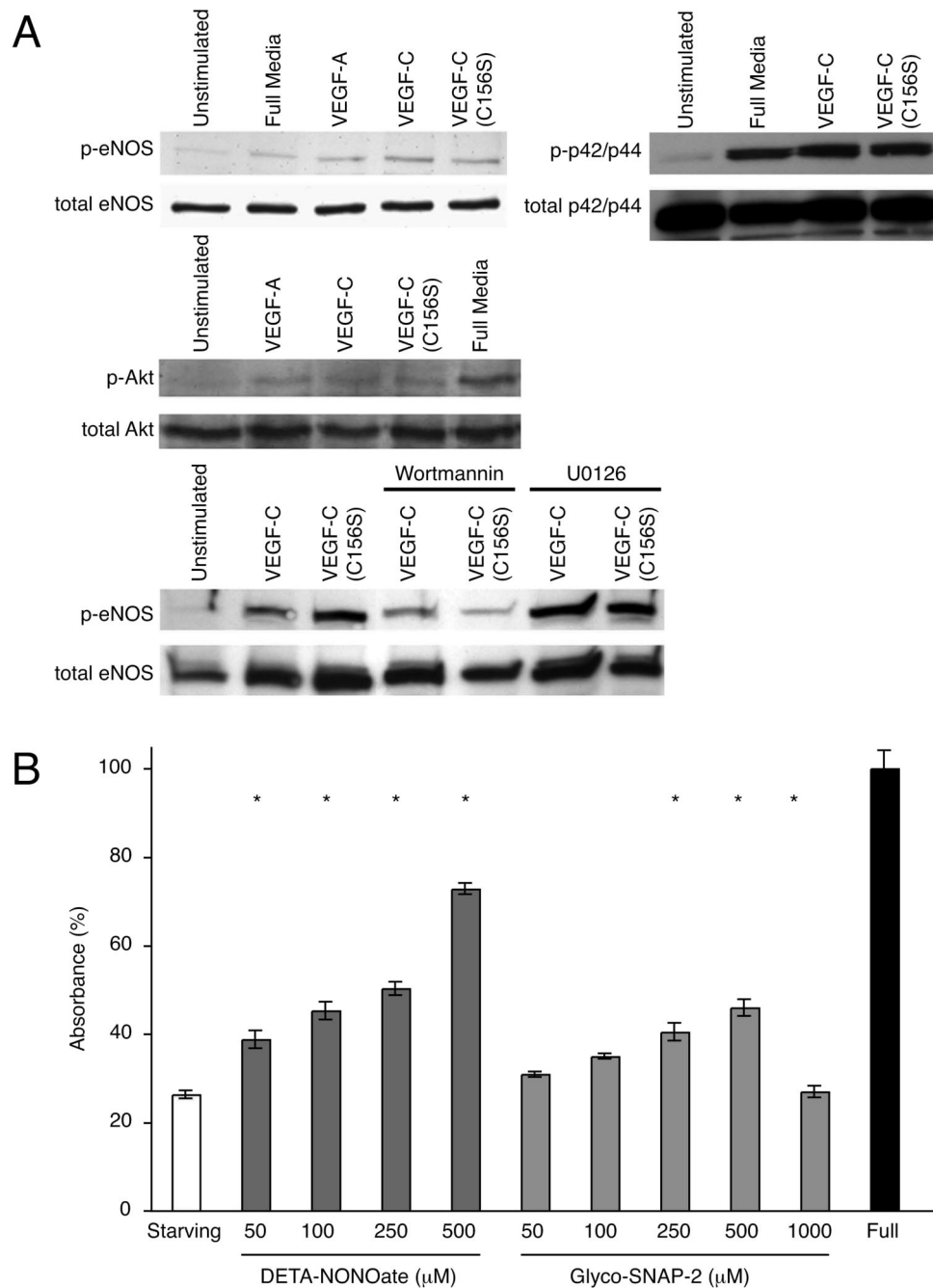


**Figure 1. eNOS activity and NO-induced proliferation of lymphatic endothelial cells**

(A) VEGF-C and VEGF-C (*C156S*) induce PI3K-dependent activation of eNOS in LECs. Signaling through VEGFR-2 and VEGFR-3 leads to activation of eNOS, Akt and p42/p44 in LECs as detected by Western blot analysis for phosphorylated eNOS (Ser1177), Akt (473) and p42/p44 (Thr202/Tyr204) proteins after LEC stimulation with VEGF-A, VEGF-C and VEGF-C (*C156S*). eNOS activation after VEGFR-2 or VEGFR-3 stimulation is dependent on PI3K activity as shown by decreased eNOS phosphorylation after pretreatment of LECs with PI3K inhibitor Wortmannin. (B) Effect of exogenous NO donors on lymphatic endothelial cell proliferation and/or survival. LEC proliferation and/or survival in response to increasing concentrations of NO donors DETA-NONOate and Glyco-SNAP-2 in growth factor reduced

media was analyzed after 72h treatment using WST-1 cell proliferation reagent. Absorbance (450nm) obtained for cells incubated with full endothelial cell growth media was set to 100%. Bars represent mean  $\pm$  SEM of quadruplicate samples. \* $P$ <0.05, Student  $t$  test.

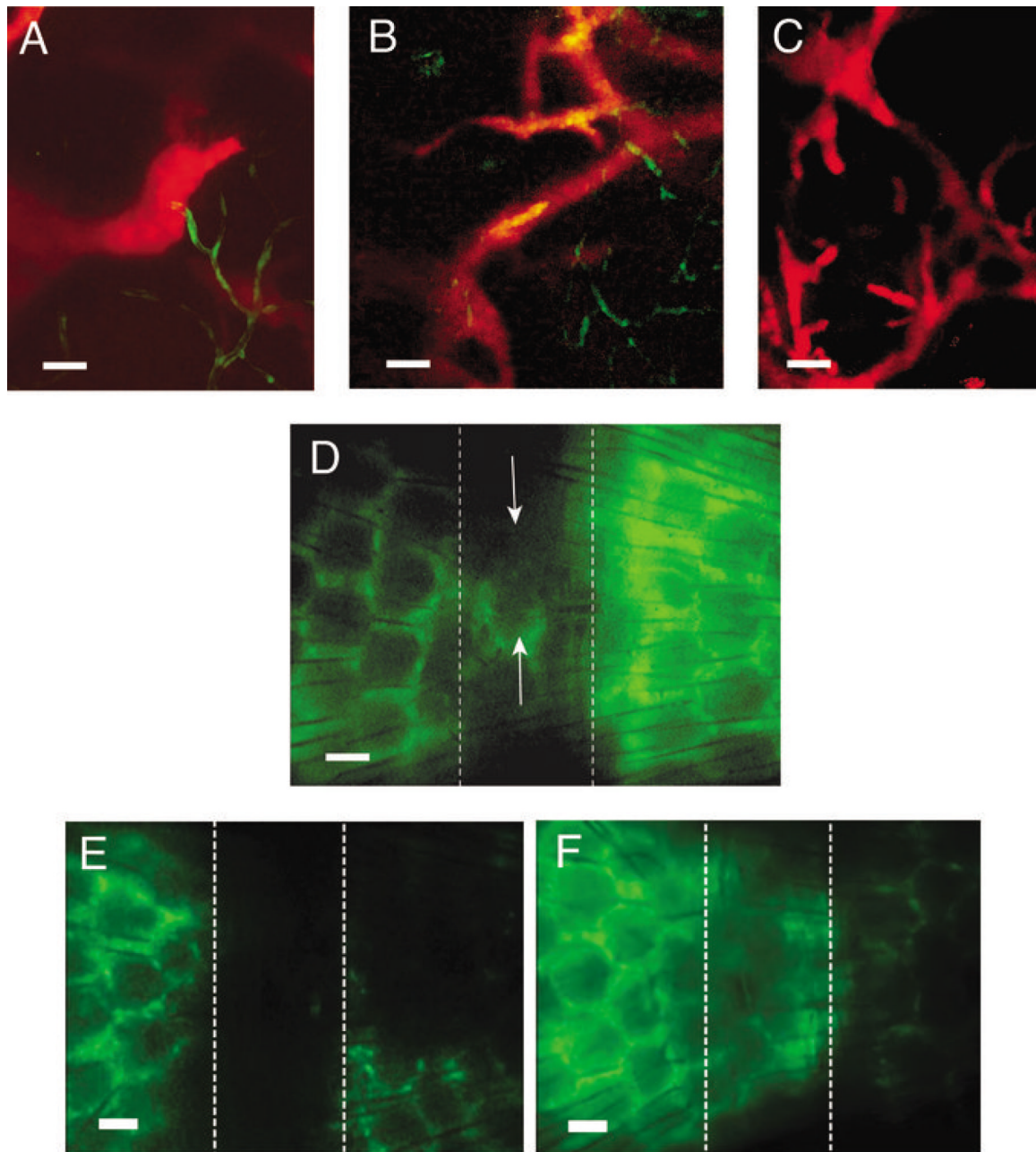


**Figure 2. Imaging of lymphangiogenesis in mouse tail dermal regeneration model**

(A) The lymphatics in normal mouse tail are imaged by lymphangiography (red) and the blood vasculature by GFP expression (green) under the control of endothelial specific Tie2 promoter. (B) Sprouting of lymphatic vessels (red) in the distal part of the collagen construct at 35 days after implantation. Direction of flow is right to left. (C) Newly regenerated lymphatics in the collagen construct 70 days after implantation. (D) The partly regenerated lymphatic network (arrows) in the collagen construct at one year after implantation. (E) L-NMMA animals 60 days after the dermal wound creation. No lymphatic regeneration was detected in the collagen construct. Animals were treated with the NOS-inhibitor L-NMMA between 21 and 60 days after the wound creation. (F) Control animals 60 days after the dermal wound creation. Lymphatics regenerated in a hexagonal pattern. Dashed lines (D-F) indicate the location of the

implanted collagen construct. Directions of lymph flow (D-F) are from left to right and the tail fills the entire field of view. Scale bars: (A-C) 50 $\mu$ m; (D-F) 200  $\mu$ m.

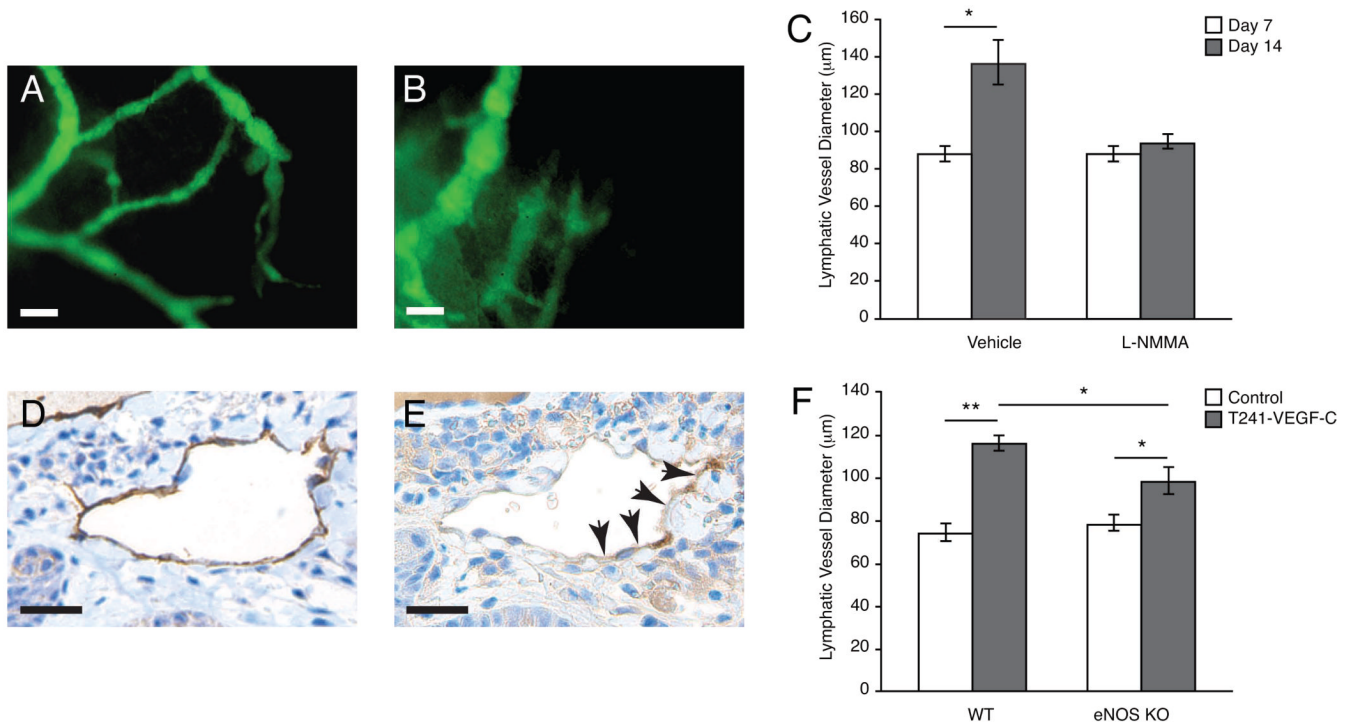


**Figure 3. Effect of pharmacologic and genetic NOS-inhibition on peritumor lymphatic hyperplasia** (A-C) Representative fluorescence images after FITC-Dextran lymphangiography. Animals received PBS or L-NMMA treatment starting on 7 days after T241-VEGF-C tumor implantation. Fourteen days after tumor implantation, lymphangiography was repeated and revealed that hyperplastic peritumor lymphatics in control animals (A) and attenuation in peritumor lymphatics hyperplasia in L-NMMA treated animals (B). (C) Quantification of the lymphatic vessel diameters after lymphangiography showed significantly reduced hyperplasia after 7 days of L-NMMA treatment. (D, E) Immunohistochemistry for LYVE-1 (D) and eNOS (E) shows that eNOS is expressed in peritumor lymphatics. Scale bars represent 100µm. (F) Rhodamine-Dextran lymphangiography revealed a significant reduction of peritumoral lymphatic hyperplasia in *eNOS*<sup>-/-</sup> mice implanted with T241-VEGF-C-GFP tumors compared to tumors implanted in wt mice. Normal ear lymphatics (control) had similar diameters. \* $P < 0.05$ , \*\* $P < 0.01$ , Student *t* test.

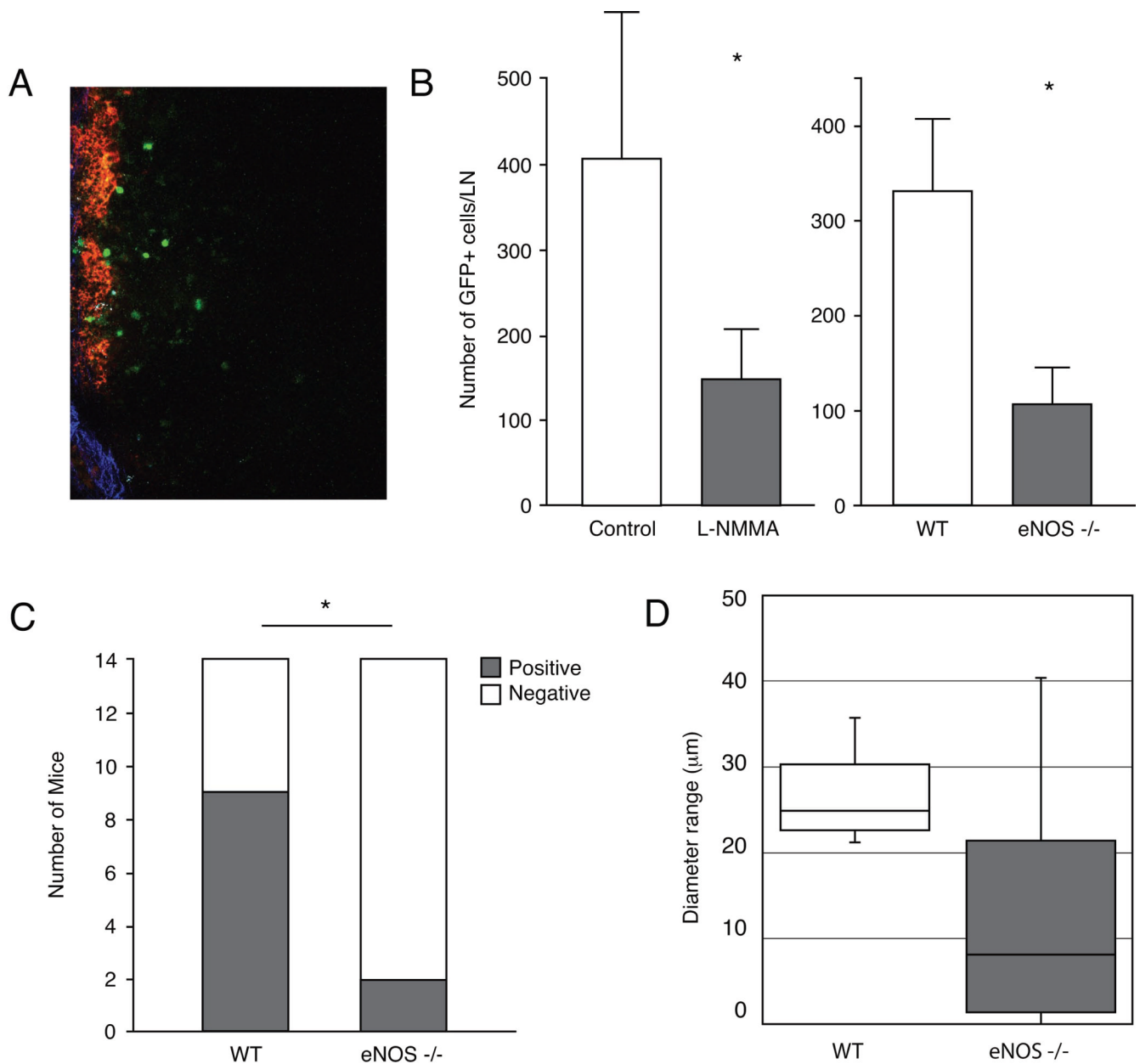


**Figure 4. Effect of pharmacologic and genetic eNOS-inhibition on lymph node metastasis**

(A) Image of a lymph node where seeded GFP+ T241-VEGF-C tumor cells can be seen in green. Red color indicates the Rhodamine-Dextran lymphangiography and the blue color indicates the collagen capsule of the lymphnode as visualized by second harmonic generation. (B) Animals received L-NMMA treatment starting 7 days after T241-VEGF-C-GFP ear tumor implantation. Fourteen days after implantation, GFP+ tumor cells in the cervical lymph node were quantified using multiphoton laser-scanning microscopy (9). L-NMMA significantly inhibited arrival of metastatic GFP+ tumor cells to the draining lymph node. Multiphoton laser-scanning microscopy also revealed a significant reduction of metastatic GFP+ tumor cell arrival to the draining lymph node 7 days after T241-VEGF-C-GFP ear tumor implantation in wt or *eNOS*<sup>-/-</sup> mice. (C) Genetic eNOS inhibition attenuates formation of clinical lymphatic metastasis. Fourteen days after B16F10 tumor implantation in mouse ears, cervical lymph

nodes were inspected for the presence of metastasis lesions. Number of metastasis was significantly reduced in *eNOS*<sup>-/-</sup> mice when compared to wt mice. **(D)** Although statistical significance was not reached, LYVE 1 immunohistochemistry showed hyperplastic B16F10 peritumor lymphatic vessels in control mice and moderately hyperplastic lymphatic vessels in *eNOS*<sup>-/-</sup> mice. \**P*<0.05, Student *t* test (A and D), Mann-Whitney-U-test (B), Fisher's exact test (C).

**Table 1**

Effect of NOS blockade on lymphatic and blood vessels in T241-VEGF-C-GFP tumors.

	Control	L-NMMA
Lymphatic vessel diameter ( $\mu\text{m}$ ) (IVM)	137 $\pm$ 12	94 $\pm$ 4*
Lymphatic vessel perimeter ( $\mu\text{m}$ ) (histology)	386 $\pm$ 27	186 $\pm$ 9*
Proliferating lymphatic endothelial cell (cells / vessel section)	3.1 $\pm$ 0.6	1.0 $\pm$ 0.6*
Blood vessel density (No. of endothelial cell nuclei per 20x field)	64 $\pm$ 11	61 $\pm$ 3
Tumor volume ( $\text{mm}^3$ )	64 $\pm$ 8	69 $\pm$ 10

Animals received L-NMMA or PBS treatment starting 7 days after VEGF-C-overexpressing T241 fibrosarcoma implantation into the mouse ear. Fourteen days after the tumor implantation, peripheral ear lymphangiography was performed followed by immunohistochemical analyses of blood vessel density, lymphatic vessel perimeter, and lymphatic endothelial cell proliferation.

\*  $p < 0.05$  as compared to the corresponding controls, Student *t* test.